Journal of Alloys and Compounds 488 (2009) 511–517

Contents lists available at ScienceDirect

Journal of Alloys and Compounds

journal homepage: www.elsevier.com/locate/jallcom

Structural chemistry and magnetic properties of $RE_2[Sn_xGe_{1-x}]_5$ (RE = Nd, Sm) and $RE[Sn_xGe_{1-x}]_2$ (RE = Gd, Tb): Four new rare-earth metal intermetallic compounds with germanium zig-zag chains and tin square-nets

Paul H. Tobash[a], Svilen Bobev[a,*], Filip Ronning[b], Joe D. Thompson[b], John L. Sarrao[b]

[a] Department of Chemistry, University of Delaware, Newark, Delaware 19716, United States
[b] Materials Physics and Application Division (MPA-10), Los Alamos National Laboratory, Los Alamos, New Mexico 87545, United States

ARTICLE INFO

Article history:
Received 16 May 2008
Received in revised form 6 October 2008
Accepted 14 October 2008
Available online 2 December 2008

Keywords:
Intermetallics
Chemical synthesis
Crystal structure
X-ray diffraction
Magnetic measurements

ABSTRACT

Four new rare-earth metal tin germanides with general formulae $RE_2[Sn_xGe_{1-x}]_5$ (RE = Nd, Sm; $x \approx 0.25$–0.3) and $RE[Sn_xGe_{1-x}]_2$ (RE = Gd, Tb; $x \approx 0.2$–0.25) have been synthesized from the corresponding elements by high temperature reactions using Sn flux. Their structures have been established from single-crystal and powder X-ray crystallography: orthorhombic space group *Cmcm* (No. 63) with cell parameters $a = 4.1057(6)$ Å, $b = 35.992(5)$ Å, $c = 4.2534(6)$ Å for $Nd_2[Sn_xGe_{1-x}]_5$; $a = 4.0707(8)$ Å, $b = 35.550(7)$ Å, $c = 4.2095(8)$ Å for $Sm_2[Sn_xGe_{1-x}]_5$; $a = 4.2248(11)$ Å, $b = 30.451(8)$ Å, $c = 4.0013(11)$ Å for $Gd[Sn_xGe_{1-x}]_2$, and $a = 4.1936(13)$ Å, $b = 30.230(9)$ Å, $c = 3.9793(12)$ Å for $Tb[Sn_xGe_{1-x}]_2$, respectively. The structures of the two families can be described as being stacking variants of the $ZrSi_2$ and $DyGe_3$ types, respectively. They represent another example of site preferences between two group 14 elements, where the lighter Ge atoms preferentially form zig-zag chains while the square sheets (or double square sheets) are made up of Sn atoms, respectively. Magnetic susceptibility measurements show that all of the compounds order antiferromagnetically at low temperatures and their respective ordering temperatures are further corroborated by specific heat measurements.

1. Introduction

Recently, we reported on a series of nearly equiatomic rare-earth metal tin germanides with a general formula $RESn_{1+x}Ge_{1-x}$ (RE = Y, Gd-Tm) [1]. In these nearly stoichiometric compounds ($x \approx 0.15$), two group 14 elements, Ge and Sn, preferentially occupy different crystallographic sites, which is a rare demonstration of site preferences between elements from the same group [2–5]. Our initial interest in this system was motivated by the success in growing single-crystals of the ternary phases RE_2InGe_2 (RE = Sm, Gd-Ho, Yb) from In flux [6], and from the speculation that intriguing physics could result if the isostructural stannides (electron-richer) could be synthesized. This line of thinking originated from the fact that computational studies on a series of compounds with the same structure type in which the RE_2InGe_2 compounds crystallize (U_3Si_2 or its ternary version Mo_2FeB_2 – space group $P4/mbm$, Pearson's symbol $tP10$) [7], suggest that the atom with the square planar coordination, In if the [$InGe_2$] layers are considered, has an oxidation state of 0 [8].

Throughout our systematic investigations of the phase space in the RE-Sn-Ge systems (RE = Ce-Tm), besides the $RESn_{1+x}Ge_{1-x}$ compounds, we came across four new ternary phases, which are the subject of this study. Their chemical formulae are $RE_2[Sn_xGe_{1-x}]_5$ ($x \approx 0.25$–0.3) for RE = Nd or Sm, and $RE[Sn_xGe_{1-x}]_2$ ($x \approx 0.2$–0.25) for RE = Gd and Tb, respectively. The structures of these new intermetallics are abbreviated hereafter as **I** and **II**, respectively, and exemplify the same site preferences mentioned above for the $RESn_{1+x}Ge_{1-x}$ (RE = Y, Gd-Tm) compounds [1], despite that they are subtly different. Herein, we discuss the results from the single-crystal X-ray diffraction work and reconcile them with periodic trends in the lanthanide family. Reported as well are the temperature dependent magnetization and specific heat measurements for all four compounds, which indicate antiferromagnetic ordering at low temperatures.

2. Experimental

2.1. Synthesis

Handling of the starting materials, pure elements from Alfa (purity > 99.9% metal basis), was done inside an argon-filled glove-box or under vacuum. Stoichiometric mixtures of the elements, used as received, were loaded in alumina crucibles, which were encapsulated in fused silica ampoules. The ampoules were evacuated (*ca.* 10^{-3} Torr) and flame-sealed. The reaction conditions were identical to those used

* Corresponding author. Tel.: +302 831 8720 fax: +302 831 6335.
E-mail address: bobev@udel.edu (S. Bobev).

0925-8388/$ – see front matter © 2008 Elsevier B.V. All rights reserved.
doi:10.1016/j.jallcom.2008.10.045

for the synthesis of the recently reported $RESn_{1+x}Ge_{1-x}$ (*RE* = Y, Gd-Tm) [1]. The only difference is that in the previous studies, the ratio *RE*:Ge was 1:1, thereby yielding nearly equiatomic compounds. In the present case, the reactions were loaded with 50% more Ge, yielding **I** and **II**, respectively. Further and more elaborate details can be found elsewhere [1].

The crystals isolated from the reactions appeared like platelets with silver-metallic luster. They are air- and moisture-stable over periods of time greater than 12 months.

2.2. X-ray diffraction studies

X-ray powder diffraction patterns were taken at room temperature on a Rigaku Miniflex powder diffractometer using filtered Cu Kα radiation. The typical scans were in $\theta-\theta$ mode ($2\theta_{max} = 80^\circ$) with a step-size of 0.05° and 10 s/step counting time. The collected powder patterns were used for phase identification only. This was done using the JADE 6.5 software package [9]. The intensities and the positions of the experimental and the calculated from the crystal structures peaks were in excellent agreement.

X-ray single-crystal data collections were carried out on a Bruker SMART CCD diffractometer at 120 K. This was necessary since the crystals were mounted on glass fibers using Paratone-N oil, which freezes at low temperature and keeps the crystals from moving. Full spheres of intensity data for multiple crystals from all compounds were collected using monochromated Mo Kα radiation. The data acquisition strategy involved batch runs at different ω and ϕ angles, which were handled using the SMART software [10]. SAINTplus [11] was used for data integration and global unit cell refinements taking into account all reflections. Semi-empirical absorption correction based on equivalents was applied with SADABS [12]. The systematic absence of reflections with indexes *hkl* for $h+k \neq 2n$; confirmed the C-centering. The presence of glide symmetry was also evident based on the observed reflection conditions, narrowing the possible choices of a space group to *Ama*2, $Cmc2_1$ and *Cmcm*—among them, the latter was favored according to the intensity statistics. The structures were solved in *Cmcm* and refined by full-matrix least-squares methods on F^2 using the SHELX package [13]. Further details of the data collection and structural refinement parameters are summarized in Table 1. In the last refinement cycles the atomic coordinates were standardized using TIDY [14]. Final positional and equivalent displacement parameters are given in Table 2 and selected bond distances are provided in Table 3. The crystallographic information files (CIF) have also been deposited with Fachinformationszentrum Karlsruhe de [76344 Eggenstein, Leopoldshafen, Germany; fax: +49 7247 808 666 email: crysdata@fiz.karlsruhe.de; depository numbers CSD-419481 ($Nd_2[Sn_xGe_{1-x}]_5$), CSD-419482 ($Sm_2[Sn_xGe_{1-x}]_5$), CSD-419483 ($Gd[Sn_xGe_{1-x}]_2$), and CSD-419484 ($Tb[Sn_xGe_{1-x}]_2$)].

We also note here that once the basic atomic arrangement in **II** was established from single-crystal work, it was found that it is similar to that in $DyGe_{1.85}$ [15] and $ErGe_{1.83}$ [16], close relatives of the common $ZrSi_2$ type [7]. However, the so-called $DyGe_{1.85}$ type is reported with the non-centrosymmetric $Cmc2_1$ space group (No. 36). It has the same reflection conditions as the centrosymmetric *Cmcm* (No. 63), making the differentiation between them virtually impossible. The same ambiguity was encountered with **I** as well. Therefore, trial-and-error solutions and refinements were carried out in both groups, but the exchange of the mirror plane with a 2_1-screw axis and the corresponding loss of inversion symmetry did not yield statistically significant improvements. The refinements showed almost no difference in the refined coordinates and both converged to very similar residuals. Because the disorder we describe in greater detail further on is persistent in both $Cmc2_1$ and *Cmcm*, and since we find no compelling geometric arguments against the inversion symmetry, we report both **I** and **II** in the higher symmetry space group *Cmcm*.

Table 2
Atomic coordinates, isotropic displacement parameters (U_{eq}) for $RE_2[Sn_xGe_{1-x}]_5$ (*RE* = Nd, Sm) and $RE[Sn_xGe_{1-x}]_2$ (*RE* = Gd, AtomTb).

Atom	Site	*x*	*y*	*z*	U_{eq} [Å^2]
$Nd_2[Sn_xGe_{1-x}]_5$					
Nd1	4*c*	0	0.44946(1)	1/4	0.0052(1)
Nd2	4*c*	0	0.85457(1)	1/4	0.0047(1)
Sn1/Ge1[a]	4*c*	0	0.21330(2)	1/4	0.0125(2)
Sn2/Ge2[a]	4*c*	0	0.28818(2)	1/4	0.0104(2)
Ge3	4*c*	0	0.07812(2)	1/4	0.0080(2)
Ge4	4*c*	0	0.62143(2)	1/4	0.0054(2)
Ge5A[b]	8*f*	0	0.00627(1)	0.074(1)	0.0050(5)
Ge5B[b]	8*f*	0	0.01249(6)	0.193(1)	0.0050(5)
$Sm_2[Sn_xGe_{1-x}]_5$					
Sm1	4*c*	0	0.44926(2)	1/4	0.0045(2)
Sm2	4*c*	0	0.85468(2)	1/4	0.0040(2)
Sn1/Ge1[a]	4*c*	0	0.21311(3)	1/4	0.0120(4)
Sn2/Ge2[a]	4*c*	0	0.28844(4)	1/4	0.0113(5)
Ge3	4*c*	0	0.07785(5)	1/4	0.0073(4)
Ge4	4*c*	0	0.62207(4)	1/4	0.0050(3)
Ge5A[b]	8*f*	0	0.0058(2)	0.067(2)	0.003(1)
Ge5B[b]	8*f*	0	0.0116(1)	0.189(2)	0.003(1)
$Gd[Sn_xGe_{1-x}]_2$					
Gd1	4*c*	0	0.44111(3)	1/4	0.0073(2)
Gd2	4*c*	0	0.66734(3)	1/4	0.0064(2)
Sn1/Ge1[a]	4*c*	0	0.24758(4)	1/4	0.0073(4)
Ge2	4*c*	0	0.09014(6)	1/4	0.0094(4)
Ge3	4*c*	0	0.85655(6)	1/4	0.0077(4)
Ge4A[b]	8*f*	0	0.0070(2)	0.097(2)	0.009(1)
Ge4B[b]	4*c*	0	0.0121(2)	1/4	0.009(1)
$Tb[Sn_xGe_{1-x}]_2$					
Tb1	4*c*	0	0.44093(3)	1/4	0.0089(2)
Tb2	4*c*	0	0.66747(3)	1/4	0.0079(2)
Sn1/Ge1[a]	4*c*	0	0.24783(5)	1/4	0.0096(4)
Ge2	4*c*	0	0.09015(7)	1/4	0.0109(4)
Ge3	4*c*	0	0.85583(7)	1/4	0.0094(4)
Ge4A[b]	8*f*	0	0.0067(2)	0.095(2)	0.009(1)
Ge4B[b]	4*c*	0	0.0117(2)	1/4	0.009(1)

[a] Refined as statistical mixtures of Sn and Ge.
[b] Disordered sites, partially occupied.

Table 1
Selected single crystal collection and refinement parameters for $RE_2[Sn_xGe_{1-x}]_5$ (*RE* = Nd, Sm) and $RE[Sn_xGe_{1-x}]_2$ (*RE* = Gd, Tb).

	I		II	
Empirical formula	$Nd_2Sn_{1.24(1)}Ge_{3.55}$	$Sm_2Sn_{1.24(1)}Ge_{3.55}$	$GdSn_{0.41(1)}Ge_{1.47}$	$TbSn_{0.40(1)}Ge_{1.47}$
Formula weight	693.53	700.82	311.85	312.39
Space group, *Z*	*Cmcm* (No. 63), *Z* = 4		*Cmcm* (No. 63), *Z* = 8	
Radiation, λ	Mo Kα, 0.71073 Å			
Temperature	120 K			
Unit cell parameters				
a (Å)	4.1057(6)	4.0707(8)	4.2248(11)	4.1936(13)
b (Å)	35.992(5)	35.550(7)	30.451(8)	30.230(9)
c (Å)	4.2534(6)	4.2095(8)	4.0013(11)	3.9793(12)
V (Å^3)	628.5(2)	609.2(2)	514.8(2)	504.5(3)
Crystal size	68 μm × 65 μm × 55 μm	54 μm × 50 μm × 42 μm	43 μm × 42 μm × 38 μm	41 μm × 32 μm × 31 μm
ρ_{calc} (g/cm^3)	7.329	7.642	8.048	8.226
μ (cm^{-1})	376.7	409.3	460.1	485.9
Data/parameter	505/35	456/35	412/28	408/28
Absorption correction method	Semi-empirical, based on equivalents			
Final *R* values[a] ($I > 2\sigma_I$)	*R*1 = 0.0196 *wR*2 = 0.0423	*R*1 = 0.0208 *wR*2 = 0.0461	*R*1 = 0.0311 *wR*2 = 0.0678	*R*1 = 0.0322 *wR*2 = 0.0647
Largest peak/hole	0.89/−1.20 e$^-$/Å^3	1.45/−1.07 e$^-$/Å^3	1.98/−1.67 e$^-$/Å^3	1.90/−2.11 e$^-$/Å^3

[a] $R1 = \Sigma||F_o| - |F_c||/\Sigma|F_o|$; $wR2 = [\Sigma[w(F_o^2 - F_c^2)^2]/\Sigma[w(F_o^2)^2]]^{1/2}$, where $w = 1/[\sigma^2F_o^2 + (A \cdot P)2 + B \cdot P]$, $P = (F_o^2 + 2F_c^2)/3$; *A* and *B*: weight coefficients.

Table 3
Selected distances (Å) in $RE_2[Sn_xGe_{1-x}]_5$ (*RE* = Nd, Sm) and $RE[Sn_xGe_{1-x}]_2$ (*RE* = Gd, Tb). The distances within the disordered chains are not included.

$Nd_2[Sn_xGe_{1-x}]_5$			$Sm_2[Sn_xGe_{1-x}]_5$		
Nd1	4× Ge3	3.118(4)	Sm1	4× Ge3	3.083(5)
	2× Ge4	3.322(8)		2× Ge4	3.297(9)
	2× Nd2	3.985(2)		2× Sm2	3.931(2)
Nd2	4× Ge4	3.079(4)	Sm2	4× Ge4	3.042(5)
	2× Sn2	3.150(7)		2× Sn2	3.112(9)
	2× Ge3	3.224(8)		2× Ge3	3.190(2)
	2× Sn1	3.239(6)		2× Sn1	3.201(8)
	2× Nd1	3.985(2)		2× Sm1	3.931(2)
Sn1[a]	Sn2	2.695(3)	Sn1[a]	Sn2	2.676(2)
	4× Sn2	2.956(3)		4× Sn2	2.929(4)
	2× Nd2	3.239(6)		2× Sm2	3.201(8)
Sn2[a]	Sn1	2.695(3)	Sn2[a]	Sn1	2.676(2)
	4× Sn1	2.956(3)		4× Sn1	2.929(4)
	2× Nd2	3.150(7)		2× Sm2	3.112(9)
Ge3	2× Ge4	2.578(8)	Ge3	2× Ge4	2.572(2)
	4× Nd1	3.118(4)		4× Sm1	3.083(5)
	2× Nd2	3.224(8)		2× Sm2	3.190(2)
Ge4	2× Ge3	2.578(8)	Ge4	2× Ge3	2.572(2)
	4× Nd2	3.079(4)		4× Sm2	3.042(5)
	2× Nd1	3.322(8)		2× Sm1	3.297(9)
$Gd[Sn_xGe_{1-x}]_2$			$Tb[Sn_xGe_{1-x}]_2$		
Gd1	4× Ge2	3.061(8)	Tb1	4× Ge2	3.039(9)
	2× Ge3	3.331(2)		2× Ge3	3.319(2)
	2× Gd2	3.861(2)		2× Tb2	3.834(2)
Gd2	4× Ge3	2.999(7)	Tb2	4× Ge3	2.975(8)
	2× Ge2	3.161(2)		2× Ge2	3.140(2)
	2× Sn1	3.230(2)		2× Sn1	3.209(2)
	2× Sn1	3.273(2)		2× Sn1	3.243(2)
	2× Gd1	3.861(2)		2× Tb1	3.834(2)
Sn1[a]	4× Sn1	2.913(6)	Sn1[a]	4× Sn1	2.894(6)
	2× Gd2	3.230(2)		2× Tb2	3.209(2)
	2× Gd2	3.273(2)		2× Tb2	3.243(2)
Ge2	2× Ge3	2.576(2)	Ge2	2× Ge3	2.574(2)
	4× Gd1	3.061(8)		4× Tb1	3.039(9)
	2× Gd2	3.161(2)		2× Tb2	3.140(2)
Ge3	2× Ge2	2.576(2)	Ge3	2× Ge2	2.574(2)
	4× Gd2	2.999(7)		4× Tb2	2.975(8)
	2× Gd1	3.331(2)		2× Tb1	3.319(2)

[a] Refined as statistical mixtures of Sn and Ge.

2.3. Magnetic and specific heat measurements

Field-cooled dc magnetization (*M*) measurements were carried out using a Quantum Design MPMS SQUID magnetometer. The measurements were taken on single-crystalline samples in the temperature range from 2 to 350 K and in an applied field (*H*) of 1000 Oe. For each sample, the susceptibility was measured with crystals aligned in parallel direction with the external field and the raw magnetization data were corrected for the holder contribution and subsequently converted to molar susceptibility ($\chi_m = M/H$). The specific heat data were measured in a Quantum Design PPMS using the thermal relaxation method within the temperature range of 2–300 K.

3. Results

3.1. Synthesis

Attempts to extend both the $RE_2[Sn_xGe_{1-x}]_5$ and the $RE[Sn_xGe_{1-x}]_2$ series to the early or late rare-earth metals were not successful. In the case of the early rare-earth metals, the cubic $RESn_3$ (*RE* = La-Pr) [7] were solely formed in the reactions; for the late rare-earth metals, the above-discussed $RESn_{1+x}Ge_{1-x}$ (*RE* = Dy-Tm) compounds were formed [1]. The same is also true even for Ge-richer reactions loaded with a nominal composition *RE*:Ge = 1:2, and/or decreasing the amount of Sn flux.

After the structures were established and the small admixture of Ge and Sn was detected, additional syntheses were undertaken in order to explore the homogeneity range. Comparison of the shifts of the lines in the corresponding powder diffraction patterns immediately confirmed the dependence of the unit cell volume on the reaction conditions. Refinements on single-crystal data provided additional evidence to suggest that there was indeed a small, but not negligible stoichiometry breadth [17]. This is the case for the structurally related $RESn_{1+x}Ge_{1-x}$ (*RE* = Y, Gd-Tm) [1], where the homogeneity range is also narrow. Nevertheless, to ascertain consistency, the very same flux-grown crystals, which were used for all physical property measurements were also used for the single-crystal X-ray data collections.

3.2. Crystal structure

Schematic representations of the structures of **I** and **II** are shown in Fig. 1. To begin our brief account, it is easy and most fitting to discuss the structures considering only the polyanionic sub-network. From this point of view, **I** can be envisioned as an alternate stacking arrangement of germanium zig-zag chains, $^1_\infty[Ge_2]$, and tin double-square sheets, $^2_\infty[Sn_2]$, where every second $^2_\infty[Sn_2]$ slab is replaced by a disordered $^1_\infty[Ge_2]$ chain. An important detail that needs to be specifically mentioned is the fact the disordered chains and the regular zig-zag chains are orthogonal (Fig. 1). This arrangement is reminiscent to that of the α-$ThSi_2$ type [7] and we can also describe the structure as being an intergrowth of α-$ThSi_2$-like and $DyGe_3$-like fragments (i.e., $REGe_2 + RESn_3 = RE_2[Sn_xGe_{1-x}]_5$). Similarly, **II** can be described as an alternate stacking arrangement of germanium zig-zag chains, $^1_\infty[Ge_2]$, and tin square sheets, $^2_\infty[Sn_2]$, where every second $^2_\infty[Sn_2]$ slab is replaced by a disordered zig-

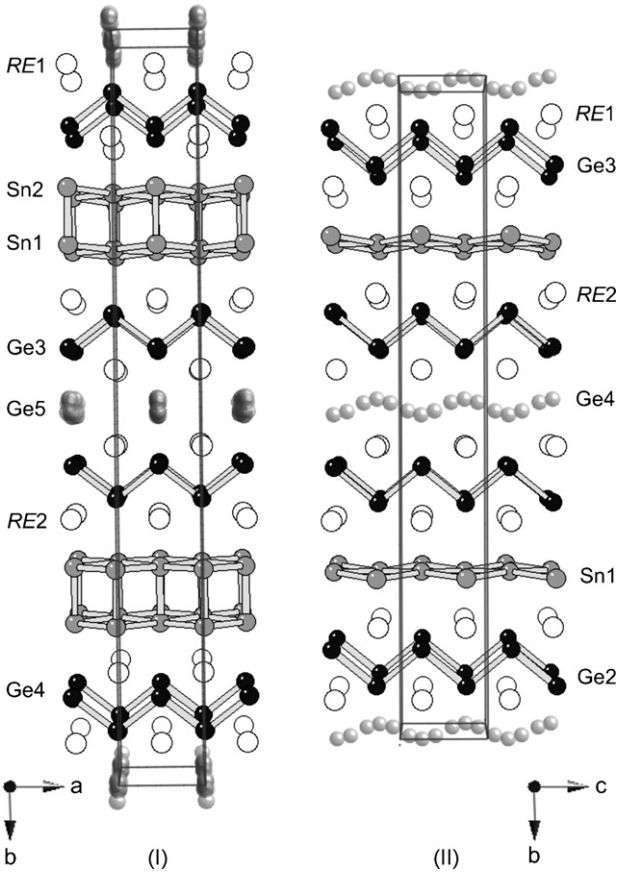

Fig. 1. The C-centered orthorhombic crystal structures of the $RE_2[Sn_xGe_{1-x}]_5$ (*RE* = Nd, Sm) (**I**) and $RE[Sn_xGe_{1-x}]_2$ (*RE* = Gd, Tb) (**II**) compounds, viewed perpendicular to the direction of the layer-stacking. Unit cells and axes directions are outlined in each case. The rare-earth metal atoms are shown as empty circles, Ge atoms are depicted as black spheres, and the Sn atoms are drawn as grey spheres. The disordered Ge-chains are shown as white spheres.

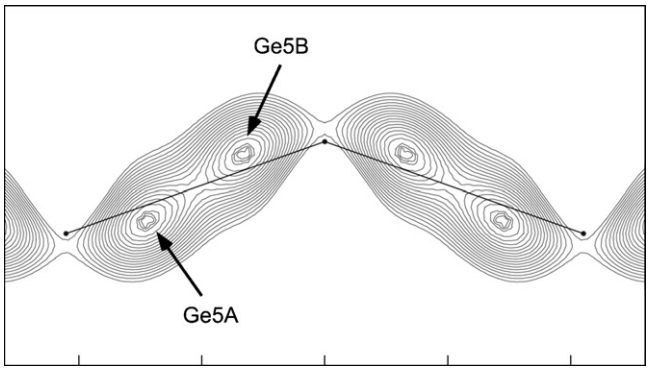

Fig. 2. Contour-diagram, calculated from the difference Fourier synthesis, showing the electron density above 5.0 e$^-$/Å^3 around the disordered Ge sites in $Sm_2[Sn_xGe_{1-x}]_5$. Similar problems persist for $Nd_2[Sn_xGe_{1-x}]_5$, as well as for $Gd[Sn_xGe_{1-x}]_2$ and $Tb[Sn_xGe_{1-x}]_2$.

zag chain. An important difference with **I** is that the disordered chains here run parallel to the neighboring $^1_\infty[Ge_2]$ groups. Thus, the $RE[Sn_xGe_{1-x}]_2$ structure can also be described as a superstructure of the $ZrSi_2$ type and is analogous to $DyGe_{1.85}$ [15] and $ErGe_{1.83}$ [16].

The Ge–Ge distances in the $^1_\infty[Ge_2]$ zig-zag chains in both families measure *ca.* 2.57 Å (Table 3) with the "corresponding" Ge-Ge-Ge angles on the order of 105° in **I** and 101° in **II**. The distances are consistent with the Ge–Ge contacts found in many other germanides: $DyGe_3$ [18], RE_3Ge_5 [19], RE_3Ge_4 [20], Yb_4MgGe_4 [21], $EuGe_2$ [22], to name a few. Turning attention to the square nets in both compounds which are composed of Sn (along with a small admixture of Ge as evidenced from the refinements), the distances measure between 2.89 and 2.95(1) Å. These are indeed longer than those found in α-Sn, but shorter than those in the metallic β-Sn allotrope [7]. They are also consistent with distances found in the square nets in $RESn_{1+x}Ge_{1-x}$ [1]. For comparison, Sn–Sn distances in the Sn sheets reported for the series of binary RE_nSn_{3n-2} compounds measure from 3.18 to 3.26 Å [23]. The interlayer distances in the double square nets in **I** measure 2.69(1) Å. Since Ge and Sn are mixed on the two sites that form this slab, it is evident why these are longer than those found in the isomorphous $DyGe_3$, $d_{Ge-Ge} = 2.44(2)$ Å [18].

The last point of relevance to this discussion concerns the disordered zig-zag chains in both structures. The disorder there is extensive and as evidenced by the difference Fourier map shown in Fig. 2, is difficult to model. These chains therefore had to be modeled by two positions (Table 2), which are with fractional occupancies. Such disorder and crystallographic approach is not without a precedent, and is reported for $ErGe_{1.83}$ [16], $LaSn_{0.75}Sb_2$ [24], and $Er_8Si_{17}B_3$ [25], among others.

3.3. Magnetic susceptibility

Plots of the magnetic susceptibility as a function of the temperature for all four $RE_2[Sn_xGe_{1-x}]_5$ (*RE* = Nd, Sm) and $RE[Sn_xGe_{1-x}]_2$ (*RE* = Gd, Tb) are shown in Fig. 3. Presented herein are the data gathered when the plate-like single-crystals used in the measurements were mounted parallel to the direction of the external field, although there were no discernable differences in the measurements in orthogonal direction. As seen from the figure, excluding $Sm_2[Sn_xGe_{1-x}]_5$, the remaining three compounds exhibit the typical Curie–Weiss paramagnetic behavior in wide temperature intervals. The cusp-like features visible in the $\chi(T)$ data are indicative of the onsets of long-range antiferromagnetic order. The corresponding Néel temperatures (T_N) were determined by taking the midpoint of the jump in $d\chi/dT$: $T_N = 5$ K for $Nd_2[Sn_xGe_{1-x}]_5$, $T_N = 13$ K for $Sm_2[Sn_xGe_{1-x}]_5$, $T_N = 25$ K for $Gd[Sn_xGe_{1-x}]_2$, and $T_N = 26$ K for $Tb[Sn_xGe_{1-x}]_2$, respectively. Below the Néel temperature, there is an upturn the $\chi(T)$ data for $Gd[Sn_xGe_{1-x}]_2$, which likely relates to the unusual C_p vs. T dependence discussed below.

The insets in Fig. 3 show the dependence of the inverse susceptibility with the temperature, which is linear in all three cases. Fitting $\chi^{-1}(T)$ yields effective moments (normalized per one *RE* atom) of $3.48\mu_B$ for the Nd-compound, $7.99\mu_B$ for the Gd-compound and $9.65\mu_B$ for the Tb-compound, respectively. These values are in very good agreement with the values calculated for free-ion Nd^{3+}, Gd^{3+} and Tb^{3+} according to the Hund's rules [26]. The negative Weiss temperatures on the order of −30 to −80 K corroborate the strong antiferromagnetic coupling in these compounds. In the case of Sm, the small effective moment along with the significant van Vleck paramagnetic contributions to the magnetization, required a non-linear fitting of the $\chi(T)$ data with the modified Curie-Weiss equation $\chi(T) = \chi_0 + C/(T - \theta_p)$ resulting in a small effective moment of $0.63\mu_B$ for Sm^{3+} and $\theta_p = -8$ K. The temperature independent contributions were estimated to be $\chi_0 = 8.8 \times 10^{-4}$ emu/mol.

3.4. Specific heat

The specific heat data are presented in Fig. 3 in the representation $C_p(T)/T$ vs. T. This is done so that a side-by-side comparison with the magnetic susceptibility can be made. In all four cases, well-defined λ-shaped peaks are seen in the plots–the temperature of the maxima correlate with the T_N's deduced from the susceptibility measurements and are characteristic of magnetically ordered systems [27]. In the case of Sm, a second anomaly near 8 K evident in the $C_p(T)$ data is also observed (Fig. 3). Its origin is unknown and could be attributed to splitting of the states for the Sm^{3+} ion, which are very close in energy, due to crystal field effects. We also note another peculiarity concerning the specific heat data for $Gd[Sn_xGe_{1-x}]_2$ (Fig. 3). Aside from the well-defined peak at 25 K, the specific heat data also shows a broad anomaly below this temperature. Similar plateau in the $C_p(T)/T$ vs. T data below the Néel temperature is also seen for $GdSn_{1+x}Ge_{1-x}$ [1], as well as for other Gd intermetallics, such as Gd_2CdPd_2 [28] and $GdNi_2Ge_2$ [29]. The nature of this effect has been suggested to originate from the coexistence of a number of commensurately and incommensurately antiferromagnetic or equal moment structures [29,30]. Currently, further studies, looking at field dependent specific heat measurements are underway.

4. Discussion

The structures of **I** and **II** are closely "rooted" from one ubiquitous structure type, CrB, which exemplifies the $^1_\infty[Ge_2]$ zig-zag chains seen here and in other *RE*Ge monogermanides [7]. As we schematically illustrate in Fig. 4, many more structures, including those of another common type, $ZrSi_2$ [7], can be "designed" by a simple "cut-and-paste" approach, where orthogonal chains or square sheets are inserted between the depicted zig-zag fragments. Starting with a CrB-like *RE*Ge monogermanide for example, and following this formalism, the simplest structure to build is that of $REGe_2$, where every other $^1_\infty[Ge_2]$ chain is replaced by a square sheet, $^2_\infty[Ge_2]$, leading to doubling of the stacking sequence and an arrangement of the $ZrSi_2$ type [7]. If every other $^1_\infty[Ge_2]$ chain is replaced by not one, but two square sheets that come in contact, i.e. double-square nets $^2_\infty[Ge_2]$, this will lead to an arrangement analogous to that in the $DyGe_3$ type [18]. Further "fine-tuning" of the latter structures by replacing every other $^2_\infty[Ge_2]$ -single or $^2_\infty[Ge_2]$ -double square sheet with different $^1_\infty[Ge_2]$ chains, will lead again

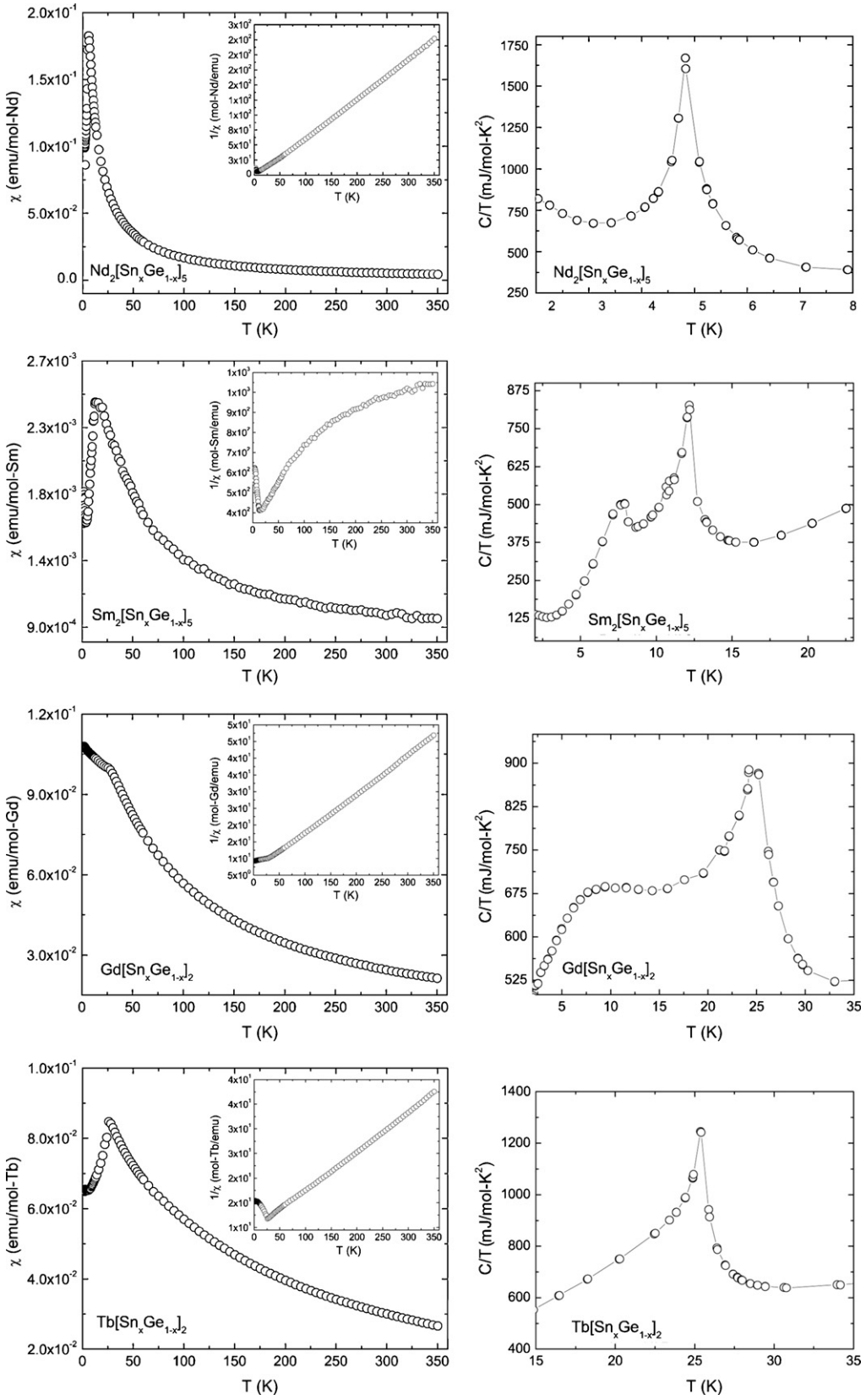

Fig. 3. Temperature dependence of the magnetic susceptibility (χ) and heat capacity (C_p) plots for $RE_2[Sn_xGe_{1-x}]_5$ (RE = Nd, Sm) and $RE[Sn_xGe_{1-x}]_2$ (RE = Gd, Tb). Inverse magnetic susceptibility $\chi^{-1}(T)$ plots are shown in the insets. The specific heat data are shown in the representation C/T vs T.

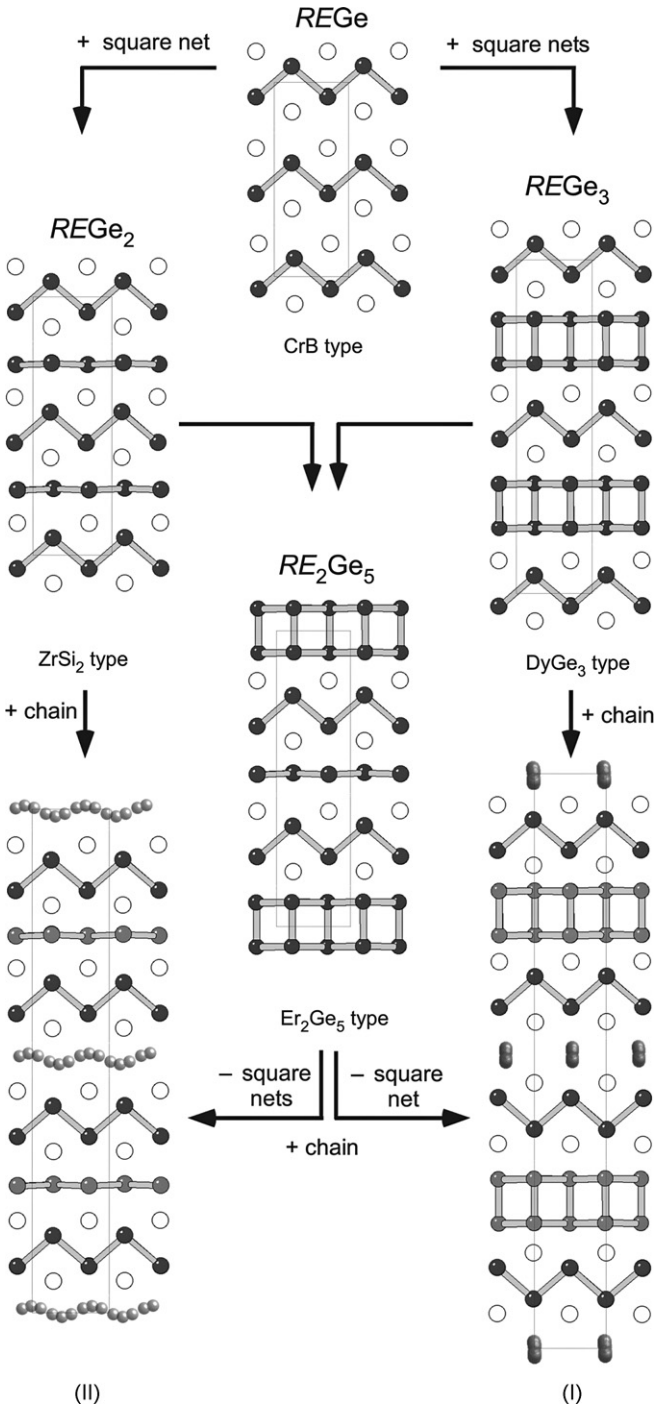

Fig. 4. Schematic representation of the way the $RE_2[Sn_xGe_{1-x}]_5$ (*RE* = Nd, Sm) and $RE[Sn_xGe_{1-x}]_2$ (*RE* = Gd, Tb) structures can be related to those of *RE*Ge (CrB type), $REGe_2$ ($ZrSi_2$ type) and $REGe_3$ ($DyGe_3$ type). Labeling of the atoms is identical to that in Fig. 1.

to doubling of the stacking sequence and structural arrangements analogous to those in **I** and **II**, respectively. It is also appropriate to mention the closely related $TmGe_{1.9}$ [31], the structure of which is composed of the same motifs except that one out of every three $^2_\infty[Ge_2]$ sheets is substituted by another Ge zig-zag chain. One can also envision various intergrowths, such as the depicted RE_2Ge_5, which is exemplified by the Er_2Ge_5 type [32]. The latter is built from three distinct moieties: (i) double square sheets, (ii) CrB type zig-zag chains, and (iii) single square sheets in an alternating arrangement. Obviously, although the overall chemical formula of the $RE_2[Sn_xGe_{1-x}]_5$ (*RE* = Nd, Sm) compounds bears resemblance to that of Er_2Ge_5, the two structures are not isotypic.

Such a design by homology allows for the prediction of new compounds and their possible structures that are likely to exist, but not yet synthesized. For instance, we can hypothesize that a possible new member of the series will be RE_3Ge_7, the structure of which is an intergrowth of $REGe_2$ and RE_2Ge_5. This particular structure is yet unknown for the *RE*–Ge systems; however, several RE_3Sn_7, the second to last members of the RE_nSn_{3n-2} (where $n = 1$–4) homologue series are already reported [23]. Although their structures are different than the ones discussed herein, a similar "building-up" approach by starting from $RESn_3$ ($AuCu_3$ type) relates the structures of all members of the family [23,33].

On this note, it also important to mention that there seems to be a size requirement not only for the *RE* metal but also for the tetrel atom, Ge or Sn, which must be met in order for a particular structure to be realized. This hypothesis is based on the observed chemical trends across the lanthanide series (see Section 2), and a previous study on the stability limits of the rare-earth metal germanides with the $ZrSi_2$- and $DyGe_3$ types [31]. It is further supported by the fact that Gd and Tb can form compounds with two distinct structures, $RESn_{1+x}Ge_{1-x}$ and $RE[Sn_xGe_{1-x}]_2$, whereas Nd and Sm seem to be able to afford only $RE_2[Sn_xGe_{1-x}]_5$. We also recall that the previously stated observation that *RE*–Ge–Sn reactions for the early lanthanides (La, Ce, Pr) result in the cubic $RESn_3$ phases and no Ge–Sn mixing [1]. These also are the very same rare-earth metals, for which the RE_nSn_{3n-2} (where $n = 1$–4) homologue series is known [23]. However, as one moves to the right of the 4*f*-block, due to the lanthanide contraction, the ionic sizes decrease and new pseudo-binary compounds with mixed Ge and Sn begin to appear [1]. Noteworthy, the mixing of these elements is not random and there seem to be preferred places for each—Ge preferentially forms zig-zag chains while Sn prefers the planar nets. It is of no surprise that the title compounds portray a "coloring effect" between two group 14 elements, Ge and Sn, being that parallel studies in the closely related $RESn_{1+x}Ge_{1-x}$ compounds also did [1]. As discussed elsewhere, rationalizing the site preferences in solids has become an integral part for understanding the reason behind why atoms arrange in a given structure [34].

Acknowledgements

Svilen Bobev acknowledges financial support from the National Science Foundation through a grant DMR-0743916 (CAREER). PHT wishes to thank the University of Delaware for the University Graduate Fellowship and the International Centre for Diffraction Data (ICDD) for the Ludo Frevel Crystallography Scholarship. Work at LANL was done under the auspices of the US DOE.

References

[1] P.H. Tobash, J.J. Meyers, G. DiFilippo, S. Bobev, F. Ronning, J.D. Thompson, J.L. Sarrao, Chem. Mater. 20 (2008) 2151.
[2] S. Ponou, T.F. Fässler, Inorg. Chem. 43 (2004) 6124.
[3] T. Kyratsi, D.Y. Chung, M.G. Kanatzidis, J. Alloys Compd. 338 (2002) 36.
[4] Y. Mozharivskyj, D. Kaczorowski, H.F. Franzen, J. Solid State Chem. 155 (2000) 259.
[5] W. Choe, G.J. Miller, J. Meyers, S. Chumbley, A.O. Pecharsky, Chem. Mater. 15 (2003) 1413.
[6] P.H. Tobash, D. Lins, S. Bobev, A. Lima, M.F. Hundley, J.D. Thompson, J.L. Sarrao, Chem. Mater. 17 (2005) 5567.
[7] P. Villars, L.D. Calvert, Pearson's Handbook of Crystallographic Data for Intermetallic Phases, second ed., American Society for Metals, Materials Park, OH, 1991.
[8] M.-H. Whangbo, C. Lee, J. Köhler, Angew. Chem. Int. Ed. 45 (2006) 7465.
[9] JADE Version 6.5, Materials Data, Inc., Livermore, CA, 2003.
[10] SMART NT, version 5.63, Bruker Analytical X-Ray Systems, Inc., Madison, WI, 2003.

[11] SAINT NT, version 6.45, Bruker Analytical X-Ray Systems, Inc., Madison, WI, 2003.
[12] SADABS NT, version 2.10, Bruker Analytical X-Ray Systems, Inc., Madison, WI, 2001.
[13] SHELXTL, version 6.12, BrukerAnalytical X-Ray Systems, Inc., Madison, WI, 2001.
[14] L.M. Gelato, E. Parthe, J. Appl. Crystallogr. 20 (1987) 139.
[15] I.R. Mokra, V.K. Pecharsky, Z.M. Shpyrka, O.I. Bodak, V.K. Belsky, I.E. Pats, Dop. AN Ukr. SSR, Ser. B 3 (1989) 48.
[16] O. Oleksyn, P. Schobinger-Papamantellos, C. Ritter, C.H. de Groot, K.H.J. Buschow, J. Alloys Compd. 252 (1997) 53.
[17] For example, crystals from $Sm_2Sn_{1.22(1)}Ge_{3.54(1)}$ were obtained from a reaction loaded with the same nominal composition as the sample listed in Table 1, but heat-treated differently. Unit cell dimensions: $a = 4.0735(9)$ Å, $b = 35.576(8)$ Å, $c = 4.2130(9)$ Å, $V = 610.5(2)$ Å^3. Similar effect on the cell constants is seen for $TbSn_{0.44(1)}Ge_{1.45(1)}$, synthesized from a reaction loaded with slightly different nominal composition and treated at the same temperature. Unit cell dimensions: $a = 4.207(3)$ Å, $b = 30.31(1)$ Å, $c = 3.995(3)$ Å, $V = 509(2)$ Å^3.
[18] P. Schobinger-Papamantellos, D.B. de Mooij, K.H.J. Buschow, J. Alloys Compd. 183 (1992) 181.
[19] P.H. Tobash, D. Lins, S. Bobev, N. Hur, J.D. Thompson, J.L. Sarrao, Inorg. Chem. 45 (2006) 7286.
[20] P.H. Tobash, G. DiFilippo, S. Bobev, N. Hur, J.D. Thompson, J.L. Sarrao, Inorg. Chem. 46 (2007) 8690.
[21] P.H. Tobash, S. Bobev, J. Am. Chem. Soc. 128 (2006) 3532.
[22] S. Bobev, E.D. Bauer, J.D. Thompson, J.L. Sarrao, G.J. Miller, B. Eck, R. Dronskowski, J. Solid State Chem. 177 (2004) 3545.
[23] F. Weitzer, K. Hiebl, P. Rogl, J. Solid State Chem. 98 (1992) 291.
[24] M.J. Ferguson, R.W. Hushagen, A. Mar, Inorg. Chem. 35 (1996) 4505.
[25] R. Jardin, V. Babizhetskyy, R. Guérin, J. Bauer, J. Alloys Compd. 353 (2003) 233.
[26] J.S. Smart, Effective Theories of Magnetism, Saunders, Philadelphia, PA, 1966.
[27] C. Kittel, Introduction to Solid State Physics, seventh ed., John Wiley and Sons, Hoboken, NJ, 1996.
[28] A. Dogan, S. Rayaprol, R. Pöttgen, J. Phys.: Condens. Matter 19 (2007) 026209.
[29] N.P. Duong, J.C.P. Klaasse, E. Brück, P.E. Brommer, F.R. de Boer, K.H.J. Bushchow, J. Magn. Magn. Mater. 262 (2003) 458.
[30] W. Good, J. Kim, A.I. Goldman, D. Wermeille, P.C. Canfield, C. Cunningham, Z. Islam, J.C. Lang, G. Srajer, I.R. Fisher, Phys. Rev. B 71 (2005) 224427.
[31] G. Venturini, J. Alloys Compd. 308 (2000) 200.
[32] G. Venturini, I. Ijjaali, B. Malaman, J. Alloys Compd. 288 (1999) 183.
[33] J.X. Boucherle, F. Givord, P. Lejay, J. Schweizer, A. Stunault, Acta Crystallogr. B44 (1988) 377.
[34] G.J. Miller, Eur. J. Inorg. Chem. 523 (1998).